

Resonant Dipole-Dipole Interactions in Electromagnetically Induced Transparency

H. H. Jen,¹ G.-D. Lin,² and Y.-C. Chen¹

¹*Institute of Atomic and Molecular Sciences, Academia Sinica, Taipei 10617, Taiwan*

²*Department of Physics, National Taiwan University, Taipei 10617, Taiwan*

(Dated: May 1, 2022)

Resonant dipole-dipole interaction (RDDI) is ubiquitous in light-matter interacting systems and is responsible for many fascinating properties of collective radiations. Here we theoretically investigate the role of RDDI in electromagnetically induced transparency (EIT). The resonant dipole-dipole interactions manifest in the cooperative spontaneous emission of the probe light transition, which give rise a broadened linewidth and associated collective frequency shift. This cooperative linewidth originates from the nonlocal and long-range RDDI, which can be determined by the atomic density, optical depth, and macroscopic length scales of the atomic ensemble. We present that EIT spectroscopy essentially demonstrates all-order multiple scattering of RDDI. Furthermore, we find that EIT transparency window becomes narrower as the cooperative linewidth increases, which essentially reduces the storage efficiency of slow light as EIT-based quantum memory application.

I. INTRODUCTION

Electromagnetically induced transparency (EIT) [1–4] has been a robust technique to store light field while preserving its quantum coherence with little dissipations. This facilitates quantum interface [5] of light and matter with high efficiency and controllability. Due to the dramatic modification of the dispersive properties accompanying with the induced transparency, the probe field propagates through the interacting medium with a reduced group velocity [6, 7]. Furthermore, the picture of dark state polariton [8] can be adopted to describe light-matter dynamics, where light can be stopped and transferred to atomic coherences, and then retrieved back to light again by turning off and on the control field. In addition to neutral atoms [3, 4, 9, 10], EIT has been implemented in various platforms including quantum degenerate gases [6, 7], Rydberg atoms [11–14], single atoms in a cavity [15, 16], embedded Fe nuclei [17], color centers in a diamond [18, 19], semiconductor quantum well [20], and crystals doped with rare-earth ions [21–25].

For EIT theory, it is mainly based on the single-particle picture within a mean field approximation. This is valid if the atomic ground state is not strongly interacting, or the energy scale of inter-atomic interaction (several hundreds of Hz in Bose Einstein condensate) is much less than the linewidth of the transition (6 MHz for D_2 transition of rubidium atoms). The theory can thus be extended to investigate many-body ground states [26, 27], which uses EIT spectroscopy to probe and extract their dynamical Green's functions [28]. On the other hand, even the atomic ground state is not strongly correlated, which is the case for cold atoms in general, single-particle picture of EIT [3, 4] neglects the effect of resonant dipole-dipole interactions (RDDIs) [29] in the dissipation channels of the coupling fields. This effect is crucial especially for atoms of high density or with a large optical depth (OD), which leads to superradiance [30, 31] and other cooperative spontaneous emissions. Therefore, single-particle EIT theory has to be extended to include the essential collective scattering events mediated by the nonlocal and long-range dipole-dipole interactions.

There has been a huge progress in recent experiments

which demonstrate the effect of dipole-dipole interactions in the radiations. These rescattering emissions between every two atoms can enhance the light emission in a dense atomic medium [32], and are responsible for subradiant emissions in neutral atoms [33], plasmonic nanocavities [34], ultracold molecules [35], and metamolecules [36]. The associated frequency shifts can also be observed in various two-level atomic systems of the embedded Fe nuclei [37], atomic vapor layer [38], ions [39], and cold atoms [40–43]. However, this evident cooperative phenomenon has been elusive in EIT platform of Λ -type atomic configuration as shown in Fig. 1. Only recently a semiclassical treatment of light-matter interactions is applied in studying EIT properties with comparable probe and control fields [44]. In this paper on the contrary, we include the RDDI in the conventional EIT theory involving up to single atomic excitation, and derive the effective linewidth broad-

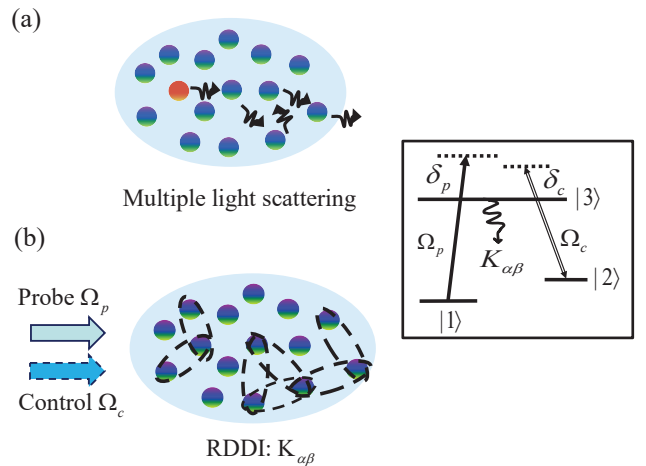


FIG. 1. Schematic plot of multiple scattering of light and EIT scheme with RDDI. (a) An excited atom emits and scatters light through many rescattering events between atoms before leaving the media and being observed. (b) A conventional EIT scheme with control Ω_c and probe fields Ω_p interacting with three-level configurations in the inset plot with the effect of pairwise RDDI $K_{\alpha\beta}$. Probe and control field detunings are denoted as δ_p and δ_c , respectively.

ening and frequency shift in EIT transmission. We show that the probe field propagates through a narrowing EIT transmission window when RDDI is significant. This reflects the non-local nature of RDDI, which incorporates all pairwise dipole-dipole interactions and can be observable in the forthcoming EIT measurements.

The paper is organized as follows. We consider a EIT scheme in an atomic ensemble and obtain the coupled equations with RDDI in Sec. II. We next investigate the linewidth of the probe light transition in Sec. III and present the results of multiple scattering of RDDI in transmission spectrum in Sec. IV. We also discuss the extension beyond the local field approximation in Sec. V. Finally we conclude in Sec. VI. In Appendix A, we introduce the Hamiltonian with RDDI and the derivations of Maxwell-Bloch equations, and in Appendix B, we present the steady-state solutions.

II. RDDI EFFECT IN EIT

In a conventional setup of EIT using Λ -type atoms in Fig. 1, a probe field Ω_p couples the ground $|1\rangle$ to the excited state $|3\rangle$ while a control field Ω_c couples $|3\rangle$ to the other hyperfine ground state $|2\rangle$. The ground state coherence establishes on absorbing a probe and emitting a control photon, which excites one of N atoms to $|2\rangle$ collectively. Therefore, a probe photon exchanging with atomic coherence forms a dark-state polariton which propagates through the medium, almost immune to the intrinsic spontaneous emission γ_{31} , and thus keeps its waveform intact inside the medium. Since light couples the atoms collectively, RDDI in the dissipation process should have an effect on EIT spectroscopy, especially for a dense atomic cloud.

Here we include and focus on the effect of RDDI in the probe transition and investigate how it modifies the conventional EIT theory. This RDDI should also manifest in the control field transition and between two ground states, with respective intrinsic decay rates γ_{32} and γ_{21} . However, a relatively large Ω_c is legitimate to neglect this effect on γ_{32} , in contrast to the weak Ω_p . The ground state decoherence also involves an inappreciable dipole transition, and therefore the effect of RDDI on γ_{21} should be insignificant compared to γ_{31} . From the Maxwell-Bloch equations we obtain in Appendix A, we have truncated the coupled equations at first-order cumulants [45] or one-body expectation values. This allows self-consistent and dynamically-coupled equations, where a hierarchy of many-body correlations are assumed insignificant. We define the cross-grained and slow-varying atomic coherence in the probe transition as $\tilde{\sigma}_{13} = N_z^{-1} \sum_{\beta=1}^{N_z} \hat{\sigma}_{13}^{\beta}(z, t) e^{i\omega_p t - i\mathbf{k}_p \cdot \mathbf{r}_{\beta}}$ with $\hat{\sigma}_{mn}^{\beta} \equiv |m\rangle_{\beta} \langle n|$, and we obtain

$$\begin{aligned} \frac{d}{d\tau} \tilde{\sigma}_{13} &\approx (i\delta_p - \gamma_{31}) \tilde{\sigma}_{13} + i \frac{\Omega_c}{2} \tilde{\sigma}_{12} + i \frac{\Omega_p}{2} \\ &\quad - \frac{1}{N_z} \sum_{\alpha=1}^{N_z} \sum_{\beta \neq \alpha}^N K_{\alpha\beta} \tilde{\sigma}_{13}^{\beta}, \end{aligned} \quad (1)$$

where $\tau = t - z/c$ in co-propagating frame, probe detun-

ing $\delta_p = \omega_p - \omega_{31}$, slow-varying atomic operator $\tilde{\sigma}_{13}^{\beta} \equiv \hat{\sigma}_{13}^{\beta} e^{i\omega_p t - i\mathbf{k}_p \cdot \mathbf{r}_{\beta}}$, and $K_{\alpha\beta} \equiv (F_{\alpha\beta} + i2G_{\alpha\beta}) e^{-i\mathbf{k}_p \cdot \mathbf{r}_{\alpha\beta}} / 2$ [29]. The RDDI of $K_{\alpha\beta}$ involves collective decay rates $F_{\alpha\beta}$ and frequency shifts $G_{\alpha\beta}$, which, at long distance, goes $\propto (|\mathbf{k}_p| r_{\mu\nu})^{-1}$ with $r_{\mu\nu} = |\mathbf{r}_{\mu} - \mathbf{r}_{\nu}|$ and wave vector of the probe field \mathbf{k}_p . The explicit forms of $F_{\alpha\beta}$ and $G_{\alpha\beta}$ can be found in Eqs. (A6) and (A7), respectively. We have assumed in Eq. (1) that all atoms are in the ground state $\tilde{\sigma}_{11} = 1$, which is valid in the linear response regime with a weak probe field. Equation (1) shows the nonlocal ($r_{\mu\nu}^{-1}$ in long range) and linear couplings between atoms throughout the medium via RDDI, in contrast to Rydberg dipole-dipole interactions ($\propto r_{\mu\nu}^{-6}$) [12, 46] where nonlinear interactions result from two or more Rydberg excitations, and a dipole-blockade sphere can be established due to large energy shift.

We then solve the steady-state ground state coherence as shown in Appendix A,

$$\tilde{\sigma}_{12} = \frac{-\Omega_c^*/2}{\delta_2 + i\gamma_{21}} \tilde{\sigma}_{13}, \quad (2)$$

where $\delta_2 = \delta_p - \delta_c$ and $\delta_c = \omega_c - \omega_{32}$ are two-photon and control-field detunings, respectively. From Eqs. (1) and (2), we iteratively solve the probe field coherence in perturbations of $K_{\alpha\beta}$ with local field approximations [46] in Appendix B.

Along with Maxwell-Bloch equation,

$$\frac{d}{dz} \Omega_p = \frac{iD\Gamma}{2L} \tilde{\sigma}_{13}, \quad (3)$$

we obtain the EIT transmission $T = |\Omega_p(L)/\Omega_p(z=0)|^2$ up to the M th order of perturbations as

$$T_M = \exp \left[\frac{D\Gamma}{2} \text{Re} \left(\sum_{m=0}^M \frac{f_C^m}{A^{m+1}} \right) \right]. \quad (4)$$

The above, as $M \rightarrow \infty$, leads to

$$T = \exp \left[\frac{D\Gamma}{2} \text{Re} \left(\frac{1}{A - f_C} \right) \right], \quad (5)$$

where

$$A \equiv i\delta_p - \gamma_{31} - \frac{i\Omega_c^2/4}{\delta_2 + i\gamma_{21}}, \quad (6)$$

$$f_C \equiv \frac{1}{N_z} \sum_{\alpha=1}^{N_z} \sum_{\beta \neq \alpha}^N K_{\alpha\beta}. \quad (7)$$

We define the optical depth as $D \equiv \rho\sigma L$ with an atomic density ρ , scattering cross section σ , and propagation length L . We further use the intrinsic decay rate $\Gamma = 2\gamma_{31}$ as a universal measure with or without RDDI. Equation (5) further indicates the effective collective frequency shift and linewidth, respectively,

$$\tilde{\delta}_p = \delta_p - \text{Im}[f_C], \quad \tilde{\gamma}_{31} = \gamma_{31} + \text{Re}[f_C], \quad (8)$$

where RDDI directly modify the transparency condition and linewidth. The transmission of Eq. (5) is valid only when

$|A| \gg |f_C|$, which is easily satisfied since $\Omega_c/|\delta_2 + i\gamma_{21}| \gg 1$ inside the transparency window or $|A| \approx |\delta_p| \gg |f_C|$ when way off single-photon resonance. Near strong absorption in EIT spectrum, that is, at small transmission T , the iterative perturbations of $K_{\alpha\beta}$ could fail since $|A| \sim \gamma_{31}$ which can be exceeded by $|f_C|$. However, for a large optical depth when $D \gg |f_C|/\gamma_{31}$, the transmission becomes vanishing, and therefore Eq. (5) still holds in this limit.

The clear advantage of EIT over fluorescence of two-level atoms on revealing cooperative linewidth manifests in the role of control field. It is this large energy scale that validates infinite (all-order) perturbations of RDDI, and thus f_C can genuinely characterize the collective frequency shift and linewidth broadening of the probe photon. On the contrary, in two-level atoms, multiple scattering of RDDI can not be quantitatively calculated unless $|f_C| \ll \gamma_{31}$, which essentially shows no cooperative effect whatsoever. To get around this issue, a direct Monte Carlo simulation can be implemented to configure atomic spatial distributions, which leads to a coupling matrix involving RDDI. Numerically diagonalizing this coupling matrix between any two radiating dipoles effectively includes all-order scattering of RDDI [32, 33]. However, this brute-force numerical method only applies well in a small Hilbert space, that is, of a small number of atoms (up to several thousands) with single [32, 33, 47] or few-photon excitations [48]. Therefore, comparing several millions of atoms operated in experiments, a huge gap nevertheless exists between theory and measurements [49], making direct comparison and prediction improbable in the near future. We note that there is a recent effort applying the concept of renormalization group method [50] to reduce the complexity of large system under strong RDDI into an ensemble of inhomogeneously broadened and weakly interacting atoms. This is the essence of cooperativity in light-matter interactions, where many-atom physics could not be easily and simply extracted from a few-atom case. This complexity even augments when nonlocal RDDI engages in the dissipation process, where atom-atom correlations are definite to play important roles [40–42] in fluorescence measurements.

III. LINEWIDTH OF PROBE LIGHT

We proceed to give an estimate of the effective linewidth f_C in Eq. (5) resulting from RDDI in Λ -type EIT scheme. f_C is defined in Eq. (7) in a form of discrete sum. First we calculate $\sum_{\beta \neq \alpha}^N K_{\alpha\beta}$ with a referenced atom at position \mathbf{r}_α , and we will prove later that the leading order result does not involve where \mathbf{r}_α is, therefore the N_z cross-grained average can just be replaced by the result of single referenced atom.

We first calculate the part of cooperative linewidth $F_{\alpha\beta}$ in f_C , and the associated frequency shift can be derived accordingly from cooperative linewidth. The continuous form of $\tilde{\gamma}_{31} = \sum_{\beta=1}^N F_{\alpha\beta} e^{-i\mathbf{k}_p \cdot \mathbf{r}_{\alpha\beta}}/2$ including the intrinsic decay

rate γ_{31} when $\beta = \alpha$ becomes [29, 51, 52]

$$\begin{aligned} \tilde{\gamma}_{31} = & N\gamma_{31} \int_{-\infty}^{\infty} dx dy dz (\pi^{3/2} R_{\perp}^{-2} R_L^{-1}) e^{-\frac{x^2+y^2}{R_{\perp}^2}} e^{-\frac{z^2}{R_L^2}} \\ & \times \int \frac{3}{8\pi} \left(1 - \frac{\sin^2 \theta}{2}\right) d\Omega_{\mathbf{k}} e^{-i\mathbf{k}_p \cdot (\mathbf{r}_\alpha - \mathbf{r})} e^{i\mathbf{k} \cdot (\mathbf{r}_\alpha - \mathbf{r})}, \end{aligned} \quad (9)$$

where we have assumed Gaussian distributions with R_{\perp} and R_L respectively for the transverse and longitudinal (propagation) length scales. The 4π solid angle integration $d\Omega_{\mathbf{k}}$ in the above comes from the original integral form of $F_{\alpha\beta}$ [29], where circular polarizations are assumed and $|\mathbf{k}| = |\mathbf{k}_p|$. We further assume \mathbf{r}_α lies on the $\hat{x} - \hat{z}$ plane with an angle θ' to \hat{z} , and we obtain

$$\begin{aligned} \tilde{\gamma}_{31} = & \int \frac{3N\gamma_{31}}{8\pi} \left(1 - \frac{\sin^2 \theta}{2}\right) \sin \theta d\theta d\phi \\ & \times e^{-|k_p|^2 R_{\perp}^2 \sin^2 \theta/4} e^{-|k_p|^2 R_L^2 (1 - \cos \theta)^2/4} \\ & \times e^{i|\mathbf{k}_p||\mathbf{r}_\alpha|(\cos \theta \cos \theta' + \sin \theta \cos \phi \sin \theta' - \cos \theta')}. \end{aligned} \quad (10)$$

We further integrate out the part of $\int d\phi$, which gives $2\pi J_0(|\mathbf{k}_p||\mathbf{r}_\alpha| \sin \theta \sin \theta')$, a Bessel function of the first kind. Since exponentially small weightings for $\theta \sim \pi/2$ in the above Gaussian functions, we consider $\theta \gtrsim 0$ and $J_0(x') \approx 1 - x'^2/4$ for small x' . We then take its leading order, set $x = \cos \theta$, and we obtain

$$\begin{aligned} \tilde{\gamma}_{31} = & \frac{3N\gamma_{31}}{8} \int_{-1}^1 (1 + x^2) dx e^{-\frac{|k_p|^2 R_{\perp}^2 (1-x^2)}{4}} e^{-\frac{|k_p|^2 R_L^2 (1-x)^2}{4}} \\ & \times e^{-i|\mathbf{k}_p||\mathbf{r}_\alpha| \cos \theta' (1-x)}. \end{aligned} \quad (11)$$

When $R_{\perp} = R_L$ and with $|\mathbf{k}_p|R_{\perp} \gg 1$, we can further simplify the above to

$$\tilde{\gamma}_{31} = \frac{3N\gamma_{31}}{8} \frac{2}{|\mathbf{k}_p|^2 R_{\perp}^2/2 + i|\mathbf{k}_p||\mathbf{r}_\alpha| \cos \theta'} \quad (12)$$

$$\approx \frac{3N\gamma_{31}}{2|\mathbf{k}_p|^2 R_{\perp}^2}. \quad (13)$$

From the above, we can express it in terms of an effective $D_c = 2\rho\sigma R_{\perp}$ with $\sigma = 3\lambda^2/(4\pi)$ and use the total volume $V = \pi^{3/2} R_{\perp}^3$ of Gaussian density distributions and the averaged density $\rho = N/V$, and we have $\tilde{\gamma}_{31}/\gamma_{31} = \sqrt{\pi} D_c/4$.

In general for a cigar shape, let $a = |\mathbf{k}_p|^2 R_{\perp}^2/4$, $b = |\mathbf{k}_p|^2 R_L^2/4$, $m \equiv b/a$, and from Eq. (11) we obtain

$$\begin{aligned} \frac{\tilde{\gamma}_{31}}{\gamma_{31}} = & \frac{3N}{8} \frac{1}{4a^{3/2}(m-1)^{5/2}} \left\{ e^{\frac{a}{m-1}} \sqrt{\pi} (4am^2 - 4ma + m \right. \\ & \left. - 1 + 2a) \left[\text{Erf} \left(\frac{(2m-1)\sqrt{a}}{\sqrt{m-1}} \right) - \text{Erf} \left(\frac{\sqrt{a}}{\sqrt{m-1}} \right) \right] \right. \\ & \left. + 2\sqrt{a}\sqrt{m-1} (e^{-4ma} - 2m + 1) \right\}, \end{aligned} \quad (14)$$

where Erf is the error function. In the extreme needle-like shape where $ma \gg 1$ and $m \gg 1$, we can further have a simple form as

$$\tilde{\gamma}_{31}/\gamma_{31} = \frac{3N}{8} \frac{\sqrt{\pi} 4am^2}{4a^{3/2} m^{5/2}} \times \frac{1}{2} = \frac{3\sqrt{\pi}}{8} \frac{N}{|\mathbf{k}_p|R_L}. \quad (15)$$

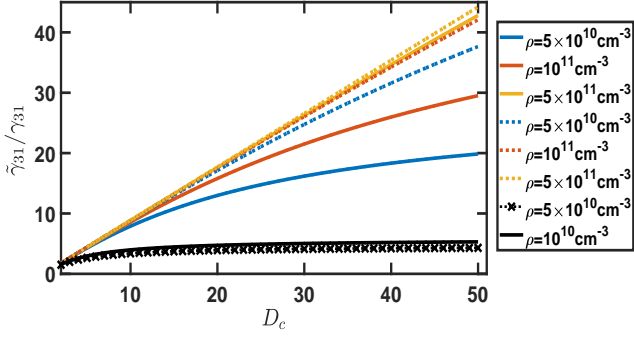


FIG. 2. Linewidth broadening from RDDI. We plot the enhanced decay rates $\tilde{\gamma}_{31}$ for various atomic densities with $R_\perp = 50$ (dot), 25 (solid), and $10 \mu\text{m}$ (\times). At relatively low atomic density, $\tilde{\gamma}_{31}$ gradually saturates as OD increases, while at large density, it approaches a linear dependence on OD . For a larger R_\perp , linewidth broadens more significantly.

Again by using the total volume $V = \pi^{3/2} R_\perp^2 R_L$ of Gaussian density distributions and the averaged density $\rho = N/V$, we derive the cooperative linewidth as

$$\tilde{\gamma}_{31}/\gamma_{31} = \frac{3\sqrt{\pi}}{8} \frac{N}{|\mathbf{k}_p| R_L} = \frac{\pi}{8} D_c \frac{|\mathbf{k}_p| R_\perp^2}{2R_L}, \quad (16)$$

where $D_c = 2\rho\sigma R_L$ is the effective optical depth. We note that the relevant parameters ρ , optical depth D_c , a total number of atom N , R_\perp , and R_L deterministically characterize the cooperative phenomena and enables a direct connection with EIT transmission measurements. These parameters are not independent from each other, since $\rho = N/V$ with $V = \pi^{3/2} R_\perp^2 R_L$ and optical depth $D_c = 2\rho\sigma R_L$.

In Fig. 2, we demonstrate $\tilde{\gamma}_{31}$ of Eq. (14) for three different R_\perp . For a fixed ρ , $\tilde{\gamma}_{31}$ saturates as D_c increases for a small ρ while approaches a linear dependence for a larger ρ . For a smaller R_\perp , $\tilde{\gamma}_{31}$ appears less significant due to small N or V involved for the cooperative linewidth at the same D_c . The interplay between R_\perp and ρ can be hardly distinguished in $\tilde{\gamma}_{31}$, which we show in the upper bounds of Fig. 2, where $\rho = 1 - 5 \times 10^{11} \text{ cm}^{-3}$ with a larger R_\perp almost overlaps with the case of $\rho = 5 \times 10^{11} \text{ cm}^{-3}$ with a halved R_\perp . We also show almost identical lower bounds, as an example, for the cases of low ρ and smaller R_\perp in Fig. 2. This reflects the difficulty in determining precise atomic configurations of N , ρ , or D_c straightforwardly from the cooperative linewidth $\tilde{\gamma}_{31}$, and therefore other complimentary and independent measurements are necessary to ensure these crucial parameters relevant to the linewidth of the probe field. As for extreme needle-like geometry, we find a suppressed $\tilde{\gamma}_{31}$ due to the factor of $|\mathbf{k}_p| R_\perp^2 / R_L$.

For cooperative frequency shift [53, 54], it is related to cooperative spontaneous decay rate, fulfilling Kramers–Kronig relations in electric susceptibility. We introduce an infrared cutoff of wave vector $k_m = 2\pi/\sqrt[3]{V}$ in calculating the cooperative frequency shift [54], and we have

$$\tilde{\delta}_p = \delta_p - \frac{2}{\sqrt{\pi}} (\tilde{\gamma}_{31} - \gamma_{31}) \frac{\lambda}{\sqrt[3]{R_\perp^2 R_L}}, \quad (17)$$

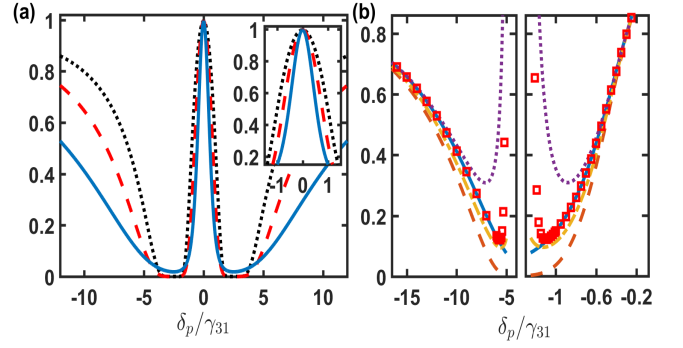


FIG. 3. EIT transmission and convergence of multiple scattering of RDDI. (a) The transmission T near two-photon resonance (inset) has shorter probe spreads from $\tilde{\gamma}_{31}/\gamma_{31} = 1$ (dot), 2 (dash) to 5 (solid), with $D_c = 20$, $\delta_c = 0$, $\Omega_c = 5\gamma_{31}$, and $\gamma_{21}/\gamma_{31} = 0.001$. The absorption peaks become broader at $|\delta_p| \gtrsim \Omega_c$ as $\tilde{\gamma}_{31}$ increases. (b) For the case of $\tilde{\gamma}_{31}/\gamma_{31} = 5$ (solid), the multiple scattering of RDDI in T_M shows convergence inside the transparency window and at off-resonance in the right and left panels respectively, with scattering orders $M = 1$ (dash), 2 (dash-dot), 3 (dot), and 20 (\square).

with a transition wavelength λ . For $R_\perp = 50 \mu\text{m}$ and $R_L = 1 \text{ mm}$, we estimate the cooperative frequency shift $\sim \tilde{\gamma}_{31}/154.2$ for a moderate atomic density we consider in Fig. 2, which has less effect than the cooperative linewidth does in EIT spectroscopy.

IV. MULTIPLE SCATTERING OF RDDI IN TRANSMISSION

Next we show the transmission T of Eq. (5) in Fig. 3 and investigate the effect of multiple scattering of RDDI. In Fig. 3(a), as $\tilde{\gamma}_{31}$ increases, the transmission window allows for shorter probe frequency spreads, and thus puts more restrictions in light propagation and reduces storage efficiency. Larger cooperative linewidth also broadens the absorption peaks. We have absorbed the cooperative frequency shifts into δ_p , which nonetheless can also be observable in conventional EIT experiments. In Fig. 3(b), we further compare the transmission with finite orders of multiple scattering of RDDI in Eq. (4). A clear convergence emerges toward higher order of perturbations, both near transparency and in the off-resonance regimes. This demonstrates that our result of transmission T from Eq. (5) essentially involves all-order scattering of RDDI, which, therefore, enables a direct comparison with present experiments. Meanwhile, close to the transmission valley (absorption peaks), a divergence shows up and the perturbation fails in this region of EIT spectrum.

Finally, in Fig. 4 we plot the FWHM of transparency window as a dependence of cooperative linewidth $\tilde{\gamma}_{31}$ for various optical depths D_c . As the optical depth increases, this bandwidth decreases as expected since in the limit of large Ω_c , it becomes

$$\sqrt{\frac{\log(2)}{2}} \frac{\Omega_c^2}{\sqrt{D_c \Gamma \tilde{\gamma}_{31}}}. \quad (18)$$

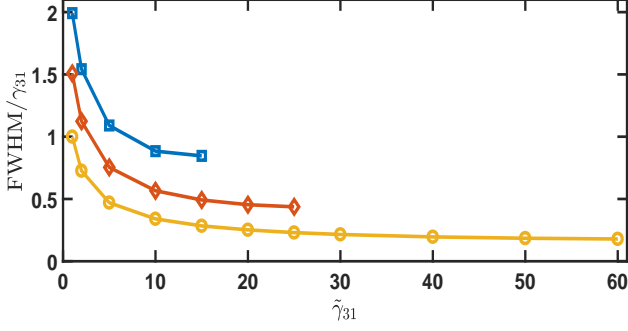


FIG. 4. Full-width-half-maximum (FWHM) of EIT transmission window. We plot the FWHM of the transparency window for $D_c = 20$ (\square), 40 (\diamond), and 100 (\circ), for various cooperative linewidth broadening $\tilde{\gamma}_{31}$. Other parameters of EIT setup are the same as Fig. 3.

In contrast, for a finite Ω_c , as the cooperative linewidth increases, the bandwidth decreases but saturates for large D_c . In Fig. 4, we stop the bandwidth calculations at a certain D_c where Eq. (5) no longer genuinely determines the FWHM of the transparency regions. Furthermore, we find a scaling of $\tilde{\gamma}_{31}^{-a}$ with $a = 0.34, 0.41,$ and 0.45 , respectively for $D_c = 20, 40,$ and 100 . This presents a significant reduction of the FWHM of EIT transmission window in a more optically thick atomic ensemble.

In contrast to Rydberg EIT experiment [12] and theory [55], the transparency is suppressed due to Rydberg dipole-dipole interactions. This nonlinear interaction results in an effective photon-photon interaction, which can be applied in realizing photonic quantum gates and forming many-body photonic bound states. On the other hand, in EIT with RDDI here, the transparency does not change significantly since no photon-photon interaction is present. What is significantly modified is the transparency bandwidth which is narrowed due to the finite cooperative linewidth. Moreover, the off-resonance absorption peaks are broadened, which can, along with the information of decreasing transparency bandwidth, further characterize the cooperative effect of RDDI in EIT.

V. BEYOND LOCAL FIELD APPROXIMATION

Here in the last section of our main results, we release the local field approximation, where multiple scattering events of RDDI can be envisaged in EIT. In practical experiments for a large optical depth, $K_{\alpha\beta}$ can be order of γ_{31} , and such that a perturbative treatment of $K_{\alpha\beta}$ is only valid when RDDI is weak in a cold gas with a low density or near the transparency regions in EIT scheme. We go beyond this approximation and proceed from Eqs. (A16) and (A18). We reevaluate the steady-state solutions still under the condition of a weak Ω_p , and so we keep only the first order of Ω_p in the Maxwell-Bloch equations of Eq. (A16).

For the first extension, we include the transverse part of field dynamics, which we will see later that it would be necessary when RDDI becomes significant. Equation (A16) be-

comes

$$\left(-\frac{i}{2k_p}\nabla_{\perp}^2 + \frac{\partial}{\partial z}\right)\Omega_p(\mathbf{r}) = \frac{iD\Gamma}{2L}\tilde{\sigma}_{13}(\mathbf{r}), \quad (19)$$

where ∇_{\perp}^2 denotes the vector Laplacian in transverse directions of \hat{x} and \hat{y} . The above presents a three-dimensional propagation equation (note that we use \mathbf{r} for the field and the dipole operator) with transverse dynamics, which takes care of refraction if there is strong RDDI.

The second extension goes to Eq. (A18), where we release the cross-section average and obtain

$$0 = \left[i\delta_p - \gamma_{31} - \frac{i|\Omega_c|^2}{4(\delta_2 + i\gamma_{21})}\right]\tilde{\sigma}_{13}^{\alpha} + i\frac{\Omega_p(\mathbf{r}_{\alpha})}{2} - \sum_{\beta \neq \alpha}^N K_{\alpha\beta}\tilde{\sigma}_{13}^{\beta}, \quad (20)$$

where we have substituted Eq. (B1). From the above, we further obtain, in discrete forms in space,

$$i\hat{M}\vec{\sigma}_{13} = -\frac{\vec{\Omega}_p}{2}, \quad (21)$$

$$\vec{\sigma}_{13} = \frac{i}{2}\hat{M}^{-1}\vec{\Omega}_p, \quad (22)$$

where $\vec{\sigma}_{13} = [\sigma_{13}(r_1), \sigma_{13}(r_2), \dots, \sigma_{13}(r_N)]$, $\vec{\Omega}_p = [\Omega_p(r_1), \Omega_p(r_2), \dots, \Omega_p(r_N)]$, and

$$M = \begin{bmatrix} -A & K_{1,2} & K_{1,3} & \dots & K_{1,N} \\ K_{2,1} & -A & K_{2,3} & \dots & K_{2,N} \\ K_{3,1} & K_{3,2} & -A & \dots & \vdots \\ \vdots & \vdots & \vdots & \ddots & K_{N-1,N} \\ K_{N,1} & \dots & \dots & K_{N,N-1} & -A \end{bmatrix}, \quad (23)$$

with $A = i\delta_p - \gamma_{31} - i|\Omega_c|^2/[4(\delta_2 + i\gamma_{21})]$ which is also defined in previous sections. From \hat{M} , we can see that the dipole operators are induced by or emerged from coupling to nonlocal fields.

With Eqs. (19) and (22) together, they describe propagation dynamics of a probe field with the effect of RDDI. By combining Eqs. (19) and (22) in continuous limit, we obtain

$$\left(-\frac{i}{2k_p}\nabla_{\perp}^2 + \frac{\partial}{\partial z}\right)\Omega_p(\mathbf{r}) = -\frac{D\Gamma}{4L}\int\hat{M}^{-1}(\mathbf{r}-\mathbf{r}')\times\Omega_p(\mathbf{r}')\rho(\mathbf{r}')d\mathbf{r}', \quad (24)$$

where $\rho(\mathbf{r})$ is the atomic density. The above results show that probe field dynamics can be influenced by RDDI in both longitudinal and transverse directions. It reduces to conventional EIT in single-particle picture when $K_{\alpha,\beta} \rightarrow 0$, leading to a local field propagation equation dominated simply by an electric susceptibility $\chi \propto A^{-1}$.

From Eq. (24), we note that a local field approximation we apply in perturbative treatments is valid only when the field is near the transparency or non-resonant regimes, that is, $\Omega_p(\mathbf{r}) \approx \Omega_p(\mathbf{r} = 0)$. Under this condition, the effect of RDDI on the effective decay rate of probe transition is most

significant, since the integral in Eq. (24) goes through all the atoms. On the other hand, when the probe field is strongly attenuated, according to Eq. (24), no significant RDDI manifests in modifying the probe field dynamics. Therefore, to determine the full EIT spectrum and associated linewidth of EIT window, a single quantity of effective decay rate is not sufficient owing to this asymmetry of regimes, especially for an atomic gas with a high optical density.

We can formally solve Eq. (24) by Laplace transforms since it has convolution forms between probe field and \hat{M}^{-1} . We then obtain (first neglecting the refraction terms and assuming a homogeneous gas $\rho = N/V$),

$$s\bar{\Omega}_p(s) - \Omega_p(z=0) = -\frac{D\Gamma}{4L}(N/L)\bar{M}^{-1}(s)\bar{\Omega}_p(s). \quad (25)$$

This gives

$$\bar{\Omega}_p(s) = \frac{\Omega_p(z=0)}{s + \frac{D\Gamma}{4L}(N/L)\bar{M}^{-1}(s)}, \quad (26)$$

which can be inverse transformed in the complex plane back to $\Omega_p(z=L)$ by

$$\Omega_p(z=L) = \frac{1}{2\pi i} \oint_{r-iR}^{r+iR} \bar{\Omega}_p(s) e^{sL} ds. \quad (27)$$

To further solve the above $\Omega_p(z=L)$, we assume again a perturbative RDDI, such that

$$M^{-1} = (-A\hat{I} + \hat{K})^{-1} \approx \frac{-1}{A} \left(1 + \frac{\hat{K}}{A} \right), \quad (28)$$

where \hat{K} represents the off-diagonal elements in Eq. (23). Now a weak RDDI can be approximated by a far-field expression in $K(r-r') \rightarrow (3\Gamma/2)(-ie^{i\xi} e^{-ik_p \cdot (r-r')})/\xi$. We finally obtain

$$\frac{\Omega_p(z=L)}{\Omega_p(z=0)} = \frac{1}{2\pi i} \oint \frac{e^{sL} ds}{s - \frac{D\Gamma}{4AL} - \frac{D\Gamma}{4AL} \left(\frac{N}{k_p L} \right) \left(\frac{3\Gamma/2}{A} \right) e^{as} \bar{\Gamma}(0, as)}, \quad (29)$$

where a is introduced in Laplace transform of $1/(|r-r'|+a)$ to remove the divergence when $r \rightarrow r'$ and is in unit of space as a complex length scale to renormalize the RDDI at divergence, and $\bar{\Gamma}$ is an incomplete Gamma function. The above is a square root of transmission, and the second term in the denominator of Eq. (29) is exactly the residue of the complex integral, leading to the EIT transmission ($T = |\Omega_p(z=L)/\Omega_p(z=0)|^2$) without RDDI,

$$\log \left(\frac{\Omega_p(z=L)}{\Omega_p(z=0)} \right) = \frac{D\Gamma}{4A}.$$

Interestingly, the third term in the denominator of Eq. (29) shows the RDDI effect leading to multiple residues in the complex plane, which indicates the failure of expressing EIT spectrum in terms of single effective decay rate. We note that these multiple scales in decay constants show up even

for a weak RDDI we consider here. In general, the multiple contributions of collective resonances and decay constants are most evident in low dimensional and dense atomic arrays, and the field propagating through constituent particles can not be genuinely described by a typical Beer-Lambert law [49] or Maxwell-Bloch equation in a macroscopic media.

VI. DISCUSSION AND CONCLUSION

Generally speaking, the RDDIs are universal in all light-matter interacting systems, which are most prominent in a dense media. They are responsible for many intriguing phenomena of superradiance and subradiance, and can be exploited to significantly enhance the performance of quantum storage efficiency in EIT under some tailored collective states [56]. Both these cooperative spontaneous emissions emerge from strong RDDIs, where multiple scattering of light exchanges between these quantum emitters dominate the dissipation process of the excited atoms.

This universal effect of RDDI should be observable as well in the EIT media, but a systematic and evident study on the collective effect from RDDI has not been reported yet or fully accounted for in most of the theoretical investigations. In terms of Langevin equations on the spontaneous emissions [57], quantum fluctuations or quantum noises play the role in initiating the dissipations of the excited atoms. Since the probe field intensity is under the normal order of field operators, it is commonly believed that the quantum fluctuations do not play a role in the probe field transmission [3, 4]. We note here that one of the crucial assumption in previous theoretical methods is the weak probe field approximation. Under this perturbation of the probe fields, up to single atomic excitation is allowed, and the collective spin excitation can form and lead to the popular picture of dark-state polariton. This picture sustains the bosonic commutation relations of the quasi-particles in large N limit and nicely explains the essential features of quantum storage and retrieval of single photon propagation in EIT media. We emphasize that this assumption can be easily broken when the light-matter interacting system goes beyond the single excitation limit when multiple excitations are present. When we have M atomic excitations in the atomic ensemble with $M \lesssim N$, naturally we face an exponential growth of the number of the states in the dynamical Hilbert space in the order of $C_M^N \sim \mathcal{O}(N^M)$ if $M \ll N$. This indicates a dilemma and challenge we would encounter in any quantum systems when a full capacity of light-matter interactions is considered in describing their system dynamics.

A relevant platform which deviates from the conventional EIT setup and has distinct EIT properties is the Rydberg EIT scheme [11–14, 58, 59]. In this platform which utilizes the high-lying Rydberg excited states, significant nonlinear effect of nonlocal dipole-dipole interactions emerge and reduce the performance of the probe field transparency. This interaction leads to the dipole blockade that forbids Rydberg excitations within the blockade radius, along with a significant energy shift away from the conventional transparency condition of two-photon resonance. Here instead we investigate the RDDI

effect in the conventional EIT setup, where the dipole-dipole interactions are induced from the light exchanges between the atomic levels of the ground and the first excited states, even though RDDIs by nature have the feature of nonlocal interaction, similar to the Rydberg EIT scheme. By contrast, the dipole-dipole interactions in Rydberg EIT media directly result from the Rydberg excited levels. The theory of Rydberg EIT takes the strategy of single-particle picture with a mean-field average of the Rydberg interactions, which results in an effective nonlocal and nonlinear interaction in EIT spectrum. Two recent studies also present a demand of a more complete understanding of Rydberg EIT system [60, 61], where radiation trapping of scattered photons [60] or emerging nontrivial photon correlations [61] might be crucial to fill the gap between the mean-field models and experiments.

In conclusion, we have theoretically investigated the role of RDDI in EIT properties. We have predicted the effective cooperative linewidth and frequency shift in EIT transmission from the multiple scattering of RDDI, which provides a direct comparison with experiment on the cooperative phenomena in EIT. The allowed transparent probe spread in the EIT transmission window is reduced due to a finite cooperative linewidth, which makes light storage less efficient in EIT-based quantum memory application. The phenomenon of RDDI in EIT should be observable in conventional EIT experiments in atoms with a moderate atomic density and optical depth.

ACKNOWLEDGMENTS

This work is supported by the Ministry of Science and Technology (MOST), Taiwan, under the Grant No. MOST-109-2112-M-001-035-MY3. H.H.J. is also grateful for support from TG 1.2 and TG 3.2 of NCTS.

Appendix A: EIT with RDDI

1. Hamiltonian and Lindblad form

The effect of RDDI in EIT can be formulated from Maxwell-Bloch equations [57]. Two hyperfine ground states $|1\rangle$ and $|2\rangle$ are coupled respectively with the probe (Ω_p) and control fields (Ω_c), with the common excited state $|3\rangle$. The Hamiltonian in interaction picture reads

$$\begin{aligned} \hat{H}_I = & \hbar\delta_p \sum_{\mu=1}^N \hat{\sigma}_{11}^{\mu} + \hbar\delta_c \sum_{\mu=1}^N \hat{\sigma}_{22}^{\mu} \\ & + \sum_{\mu=1}^N \left(-\frac{\hbar\Omega_p}{2} e^{i\mathbf{k}_p \cdot \mathbf{r}_{\mu}} \hat{\sigma}_{13}^{\mu,\dagger} + h.c. \right) \\ & + \sum_{\mu=1}^N \left(-\frac{\hbar\Omega_c}{2} e^{i\mathbf{k}_c \cdot \mathbf{r}_{\mu}} \hat{\sigma}_{23}^{\mu,\dagger} + h.c. \right), \end{aligned} \quad (\text{A1})$$

where the wave vectors of the fields are \mathbf{k}_p and \mathbf{k}_c with the Rabi frequencies Ω_p and Ω_c respectively, and the atomic

dipole operators are $\hat{\sigma}_{ij}^{\beta} \equiv |i\rangle_{\beta}\langle j|$, $\hat{\sigma}_{ij}^{\beta,\dagger} \equiv \hat{\sigma}_{ji}^{\beta}$. The detunings are defined as $\delta_p = \omega_p - \omega_{31}$ and $\delta_c = \omega_c - \omega_{32}$, where the central frequencies of light fields are ω_p , ω_c , and the atomic transition frequencies are ω_{31} , ω_{32} .

The spontaneous emissions can be expressed in a Lindblad form [62], such that the Heisenberg equations for arbitrary operators \hat{Q} become

$$\begin{aligned} \frac{d\hat{Q}}{dt} = & -\frac{i}{\hbar} [\hat{Q}, \hat{H}_I] - i \sum_{\mu \neq \nu, \nu}^N [\hat{Q}, G_{\mu\nu} \hat{\sigma}_{31}^{\mu} \hat{\sigma}_{13}^{\nu}] \\ & + \mathcal{L}_p[\hat{Q}] + \mathcal{L}_c[\hat{Q}] + \mathcal{L}_g[\hat{Q}], \end{aligned} \quad (\text{A2})$$

where

$$\mathcal{L}_p[\hat{Q}] \equiv - \sum_{\mu, \nu}^N \frac{F_{\mu\nu}}{2} (\hat{\sigma}_{31}^{\mu} \hat{\sigma}_{13}^{\nu} \hat{Q} + \hat{Q} \hat{\sigma}_{31}^{\mu} \hat{\sigma}_{13}^{\nu} - 2\hat{\sigma}_{31}^{\mu} \hat{Q} \hat{\sigma}_{13}^{\nu}), \quad (\text{A3})$$

$$\mathcal{L}_c[\hat{Q}] \equiv - \sum_{\mu, \nu}^N \gamma_{32} (\hat{\sigma}_{32}^{\mu} \hat{\sigma}_{23}^{\nu} \hat{Q} + \hat{Q} \hat{\sigma}_{32}^{\mu} \hat{\sigma}_{23}^{\nu} - 2\hat{\sigma}_{32}^{\mu} \hat{Q} \hat{\sigma}_{23}^{\nu}), \quad (\text{A4})$$

$$\mathcal{L}_g[\hat{Q}] \equiv - \sum_{\mu, \nu}^N \gamma_{21} (\hat{\sigma}_{21}^{\mu} \hat{\sigma}_{12}^{\nu} \hat{Q} + \hat{Q} \hat{\sigma}_{21}^{\mu} \hat{\sigma}_{12}^{\nu} - 2\hat{\sigma}_{21}^{\mu} \hat{Q} \hat{\sigma}_{12}^{\nu}). \quad (\text{A5})$$

Various coherence decay rates are γ_{31} , γ_{21} , γ_{32} , and here we consider the RDDI effect in the probe transition only, whereas in the control field coupling, it is negligible due to large Ω_c and vanishing populations in $|2\rangle$ and $|3\rangle$. For the ground state decoherence, we neglect its RDDI effect as well due to the energy scale γ_{21} is irrelevant in EIT probe property.

The cooperative spontaneous decay rates $F_{\mu\nu}$ and frequency shifts $G_{\mu\nu}$ can be expressed as [29]

$$\begin{aligned} F_{\mu\nu}(\xi) \equiv & \frac{3\Gamma}{2} \left\{ \left[1 - (\hat{d} \cdot \hat{r}_{\mu\nu})^2 \right] \frac{\sin \xi}{\xi} \right. \\ & \left. + \left[1 - 3(\hat{d} \cdot \hat{r}_{\mu\nu})^2 \right] \left(\frac{\cos \xi}{\xi^2} - \frac{\sin \xi}{\xi^3} \right) \right\}, \end{aligned} \quad (\text{A6})$$

$$\begin{aligned} G_{\mu\nu}(\xi) \equiv & \frac{3\Gamma}{4} \left\{ - \left[1 - (\hat{d} \cdot \hat{r}_{\mu\nu})^2 \right] \frac{\cos \xi}{\xi} \right. \\ & \left. + \left[1 - 3(\hat{d} \cdot \hat{r}_{\mu\nu})^2 \right] \left(\frac{\sin \xi}{\xi^2} + \frac{\cos \xi}{\xi^3} \right) \right\}, \end{aligned} \quad (\text{A7})$$

where $\Gamma = 2\gamma_{31} \equiv \omega_{31}^3 d^2 / (3\pi\epsilon_0 \hbar c^3)$, is the intrinsic decay rate, and \hat{d} is the dipole orientation with dipole moment d . The dimensionless scale of mutual separation is $\xi = |\mathbf{k}_p| r_{\mu\nu}$ with $r_{\mu\nu} = |\mathbf{r}_{\mu} - \mathbf{r}_{\nu}|$. The above indicates the long-range nature of dipole-dipole interactions, which is responsible for the cooperative radiations of superradiance or subradiance. As $\xi \rightarrow 0$, $F_{\mu\nu}$ approaches Γ while $G_{\mu\nu}$ becomes divergent, showing an incomplete quantum optical treatment in this limit. For $\xi \gg 2\pi$ or $r_{\mu\nu} \gg \lambda$ (transition wavelength), both cooperative decay rates and frequency shifts diminish, which reaches the noninteracting regime of independent atoms.

2. Maxwell-Bloch equations

In this section, we derive the equations of motion for EIT with cooperative effects in the probe transition. We first define the slow-varying coherence operators as

$$\tilde{\sigma}_{13}(z, t) = \frac{1}{N_z} \sum_{\beta=1}^{N_z} \hat{\sigma}_{13}^{\beta}(z, t) e^{i\omega_p t - i\mathbf{k}_p \cdot \mathbf{r}_{\beta}}, \quad (\text{A8})$$

$$\tilde{\sigma}_{23}(z, t) = \frac{1}{N_z} \sum_{\beta=1}^{N_z} \hat{\sigma}_{23}^{\beta}(z, t) e^{i\omega_c t - i\mathbf{k}_c \cdot \mathbf{r}_{\beta}}, \quad (\text{A9})$$

$$\tilde{\sigma}_{12}(z, t) = \frac{1}{N_z} \sum_{\beta=1}^{N_z} \hat{\sigma}_{12}^{\beta}(z, t) e^{i\Delta\omega t - i\Delta\mathbf{k} \cdot \mathbf{r}_{\beta}}, \quad (\text{A10})$$

where $\Delta\mathbf{k} = \mathbf{k}_p - \mathbf{k}_c$, and $\Delta\omega = c|\Delta\mathbf{k}|$. Same cross section average is applied for the population operators,

$$\tilde{\sigma}_{11} = \frac{1}{N_z} \sum_{\beta=1}^{N_z} \hat{\sigma}_{11}^{\beta}(z, t), \quad \tilde{\sigma}_{22} = \frac{1}{N_z} \sum_{\beta=1}^{N_z} \hat{\sigma}_{22}^{\beta}(z, t),$$

$$\tilde{\sigma}_{33} = \frac{1}{N_z} \sum_{\beta=1}^{N_z} \hat{\sigma}_{33}^{\beta}(z, t).$$

These cross-grained averages of the slow-varying variables are typical treatments in solving the propagating quantized electric fields through an atomic medium. Later for predictions of EIT properties, we shall not encounter the effect from cross-grained details, which is true since we take N and $N_z \rightarrow \infty$. In the following, we will consider only one-body atomic operators in the dynamically light-matter coupled equations, which truncates the hierarchy of the equations and equivalently neglects small higher order multi-atom correlations.

In the co-propagating frame $\tau = t - z/c$, we obtain the Maxwell-Bloch equations as

$$\frac{d}{d\tau} \tilde{\sigma}_{23} = (i\delta_c - \gamma_{21} - \gamma_{32}) \tilde{\sigma}_{23} + i\frac{\Omega_c}{2} (\tilde{\sigma}_{22} - \tilde{\sigma}_{33}) + i\frac{\Omega_p}{2} \tilde{\sigma}_{12}^{\dagger}, \quad (\text{A11})$$

$$\frac{d}{d\tau} \tilde{\sigma}_{13} = (i\delta_p - \gamma_{31}) \tilde{\sigma}_{13} + i\frac{\Omega_c}{2} \tilde{\sigma}_{12} + i\frac{\Omega_p}{2} (\tilde{\sigma}_{11} - \tilde{\sigma}_{33}) - \frac{1}{N_z} \sum_{\alpha=1}^{N_z} \sum_{\beta \neq \alpha}^N K_{\alpha\beta} (\tilde{\sigma}_{11}^{\alpha} - \tilde{\sigma}_{33}^{\alpha}) \tilde{\sigma}_{13}^{\beta}, \quad (\text{A12})$$

$$\frac{d}{d\tau} \tilde{\sigma}_{12} = (i\delta_2 - \gamma_{21}) \tilde{\sigma}_{12} - i\frac{\Omega_p}{2} \tilde{\sigma}_{23}^{\dagger} + i\frac{\Omega_c^*}{2} \tilde{\sigma}_{13}, \quad (\text{A13})$$

$$\frac{d}{d\tau} \tilde{\sigma}_{11} = 2\gamma_{31} \tilde{\sigma}_{33} + 2\gamma_{21} \tilde{\sigma}_{22} - i\frac{\Omega_p}{2} \tilde{\sigma}_{13}^{\dagger} + i\frac{\Omega_p^*}{2} \tilde{\sigma}_{13} + \frac{1}{N_z} \sum_{\alpha=1}^{N_z} \sum_{\beta \neq \alpha}^N \left[K_{\alpha\beta} (\tilde{\sigma}_{31}^{\alpha} \tilde{\sigma}_{13}^{\beta}) + K_{\alpha\beta}^* (\tilde{\sigma}_{31}^{\beta} \tilde{\sigma}_{13}^{\alpha}) \right], \quad (\text{A14})$$

$$\frac{d}{d\tau} \tilde{\sigma}_{33} = -\gamma_3 \tilde{\sigma}_{33} + i\frac{\Omega_p}{2} \tilde{\sigma}_{13}^{\dagger} - i\frac{\Omega_p^*}{2} \tilde{\sigma}_{13} + i\frac{\Omega_c}{2} \tilde{\sigma}_{23}^{\dagger} - i\frac{\Omega_c^*}{2} \tilde{\sigma}_{23} - \frac{1}{N_z} \sum_{\alpha=1}^{N_z} \sum_{\beta \neq \alpha}^N \left[K_{\alpha\beta} (\tilde{\sigma}_{31}^{\alpha} \tilde{\sigma}_{13}^{\beta}) + K_{\alpha\beta}^* (\tilde{\sigma}_{31}^{\beta} \tilde{\sigma}_{13}^{\alpha}) \right], \quad (\text{A15})$$

$$\frac{d}{dz} \Omega_p = \frac{iD\Gamma}{2L} \tilde{\sigma}_{13}, \quad (\text{A16})$$

where $K_{\alpha\beta} \equiv (F_{\alpha\beta} + i2G_{\alpha\beta}) e^{-i\mathbf{k}_p \cdot \mathbf{r}_{\alpha\beta}/2}$ [29]. The slow-varying atomic operators, not the cross-grained ones, are denoted as $\tilde{\sigma}_{\mu\nu}^{\beta}$, and for example, $\tilde{\sigma}_{13}^{\beta} = \hat{\sigma}_{13}^{\beta} e^{i\omega_p t - i\mathbf{k}_p \cdot \mathbf{r}_{\beta}}$. The optical depth is $D \equiv \rho\sigma L$ and $\gamma_3 = 2\gamma_{31} + 2\gamma_{32}$. The two-photon detuning is $\delta_2 = \delta_p - \delta_c$. The RDDI in the probe transition modifies the transition coherence $\tilde{\sigma}_{13}$ and redistributes the populations of $\tilde{\sigma}_{11}$ and $\tilde{\sigma}_{33}$ through multi-atom correlations.

In this Λ -type atomic system, we assume all N atoms are initially prepared in $|1\rangle$. In the limit of weak probe field, which corresponds to a linear dependence of Ω_p in the coupled equations, we have $\tilde{\sigma}_{11} = 1$, $\tilde{\sigma}_{22} = \tilde{\sigma}_{33} = 0$, and $\tilde{\sigma}_{23} = 0$. The relevant equations for atomic coherences (with implicit spatial

dependence of z) are

$$\frac{d}{d\tau} \tilde{\sigma}_{12} \approx (i\delta_2 - \gamma_{21}) \tilde{\sigma}_{12} + i\frac{\Omega_c^*}{2} \tilde{\sigma}_{13}, \quad (\text{A17})$$

$$\begin{aligned} \frac{d}{d\tau} \tilde{\sigma}_{13} \approx & (i\delta_p - \gamma_{31}) \tilde{\sigma}_{13} + i\frac{\Omega_c}{2} \tilde{\sigma}_{12} + i\frac{\Omega_p}{2} \\ & - \frac{1}{N_z} \sum_{\alpha=1}^{N_z} \sum_{\beta \neq \alpha}^N K_{\alpha\beta} \tilde{\sigma}_{13}^{\beta}. \end{aligned} \quad (\text{A18})$$

Appendix B: Steady state solutions

Here we proceed to solve the steady-state solutions of the coupled equations in Appendix A. 2 and present how the effect of RDDI modifies the EIT spectrum. The steady state solution

of the ground state coherence from Eq. (A17) gives

$$\tilde{\sigma}_{12} = \frac{-\Omega_c^*/2}{\delta_2 + i\gamma_{21}} \tilde{\sigma}_{13}. \quad (\text{B1})$$

We then substitute $\tilde{\sigma}_{12}$ from the above in Eq. (A18), and in the zeroth order of $K_{\alpha\beta}$, for a real constant Ω_c , we derive the coherence of the probe transition (now retrieving the spatial dependence for clarity)

$$\tilde{\sigma}_{13}^{(0)}(z) = \frac{-i\Omega_p(z)/2}{i\delta_p - \gamma_{31} - \frac{i\Omega_c^2/4}{\delta_2 + i\gamma_{21}}} \equiv \frac{-i\Omega_p(z)/2}{A}, \quad (\text{B2})$$

which is proportional to the electric field susceptibility in conventional EIT theory without cooperative effects. We define A above for later concise representation of the cooperative effect on the linewidth of EIT spectrum.

Next for the first-order perturbation of $K_{\alpha\beta}$, we apply the zeroth order results of Eq. (B2) to Eq. (A18) and obtain

$$\tilde{\sigma}_{13}^{(1)}(z) = \frac{-i\Omega_p(z)/2}{A} + \frac{1}{AN_z} \sum_{\alpha=1}^{N_z} \sum_{\beta \neq \alpha}^N K_{\alpha\beta} \tilde{\sigma}_{13}^{\beta,(0)}(\mathbf{r}_\beta), \quad (\text{B3})$$

where a coupling between the atomic coherences at z and other positions $\mathbf{r}_\beta \neq \mathbf{r}_\alpha$ appears due to RDDI. Equation (B3) essentially describes nonlocal interactions of the fields. We proceed to apply the local field approximation to Eq. (B3) and obtain

$$\tilde{\sigma}_{13}^{(1)}(z) = \frac{-i\Omega_p(z)/2}{A} + \frac{f_C}{A} \frac{-i\Omega_p(z)/2}{A}, \quad (\text{B4})$$

where $f_C = N_z^{-1} \sum_{\alpha=1}^{N_z} \sum_{\beta \neq \alpha}^N K_{\alpha\beta}$ denotes the cooperative dipole-dipole interactions between the cross-grained region and all the other atoms in the ensemble. We calculate the leading order of f_C in the main paper, which is independent of the cross-grained region and is cooperatively enhanced due to the involvement of all N atoms of the medium.

From light propagation of Eq. (A16) in the Maxwell-Bloch equations, we replace the above $\tilde{\sigma}_{13}$ with $\tilde{\sigma}_{13}^{(1)}(z)$ of Eq. (B4), and $\Omega_p(L)$ becomes

$$\log \left(\frac{\Omega_p(L)}{\Omega_p(0)} \right) = \frac{D\Gamma}{4} \left(\frac{1}{A} + \frac{f_C}{A^2} \right) \approx \frac{D\Gamma}{4} \frac{1}{A - f_C}, \quad (\text{B5})$$

where the approximate form in the above is valid when $|f_C| \ll |A|$, and it suggests that there is an effective $\tilde{\delta}_p^{(1)}$ and $\tilde{\gamma}_{31}^{(1)}$ in A , which are

$$\tilde{\delta}_p^{(1)} = \delta_p - \text{Im}[f_C], \quad \tilde{\gamma}_{31}^{(1)} = \gamma_{31} + \text{Re}[f_C]. \quad (\text{B6})$$

These represent a cooperative frequency shift in δ_p and linewidth broadening (larger than γ_{31}) respectively, and their superscripts denote the single scattering event of RDDI.

To account for the multiple scattering effect in EIT theory, similar to the treatment of coherent scattering of two-level atoms [63–65], we obtain the steady state solutions of Eq. (A18) by considering a second-order perturbation, which reads

$$0 = A\tilde{\sigma}_{13}^{(2)} + \frac{i\Omega_p}{2} - f_C\tilde{\sigma}_{13}^{(1)}. \quad (\text{B7})$$

From the above and using the result of $\tilde{\sigma}_{13}^{(1)}$, we have

$$\tilde{\sigma}_{13}^{(2)} = \frac{-i\Omega_p}{2} \left[\frac{1}{A} + \frac{f_C}{A^2} + \frac{f_C^2}{A^3} \right]. \quad (\text{B8})$$

Again from Eq. (A16), we obtain the output field,

$$\log \left(\frac{\Omega_p(L)}{\Omega_p(0)} \right) = \frac{D\Gamma}{4L} \int_0^L dz \left[\frac{1}{A} + \frac{f_C}{A^2} + \frac{f_C^2}{A^3} \right], \quad (\text{B9})$$

$$\approx \frac{D\Gamma}{4} \frac{1}{A - f_C},$$

where the approximate form can be derived from the first line by using Taylor expansion, $(1 - x)^{-1} = \sum_{n=0}^{\infty} x^n$ for $x < 1$.

-
- [1] S. E. Harris, J. Field, and A. Imamoglu, Phys. Rev. Lett. **64**, 1107 (1990).
[2] S. E. Harris, Physics Today **50**, 36 (1997).
[3] M. D. Lukin, Rev. Mod. Phys. **75**, 457 (2003).
[4] M. Fleischhauer, A. Imamoglu, and J. P. Marangos, Rev. Mod. Phys. **77**, 633 (2005).
[5] K. Hammerer, A. S. Sørensen, and E. S. Polzik, Rev. Mod. Phys. **82**, 1041 (2010).
[6] L. V. Hau, S. E. Harris, Z. Dutton, and C. H. Behroozi, Nature **397**, 594 (1999).
[7] U. Schnorrberger, J. D. Thompson, S. Trotzky, R. Pugatch, N. Davidson, S. Kuhr, and I. Bloch, Phys. Rev. Lett. **103** 033003 (2009).
[8] M. Fleischhauer and M. D. Lukin, Phys. Rev. A **65**, 022314 (2002).
[9] Y.-F. Hsiao, P.-J. Tsai, H.-S. Chen, S.-X. Lin, C.-C. Hung, C.-H. Lee, Y.-H. Chen, Y.-F. Chen, A. Y. Ite, and Y.-C. Chen, Phys. Rev. Lett. **120**, 183602 (2018).
[10] Y. Wang, J. Li, S. Zhang, K. Su, Y. Zhou, K. Liao, S. Du, H. Yan, and S.-L. Zhu, Nat. Photon. **13**, 346 (2019).
[11] M. Saffman and T. G. Waller, Rev. Mod. Phys. **82**, 2313 (2010).
[12] J. D. Pritchard, D. Maxwell, A. Gauguier, K. J. Weatherill, M. P. A. Jones, C. S. Adams, Phys. Rev. Lett. **105**, 193603 (2010).
[13] Y. O. Dudin and A. Kuzmich, Science **336**, 887 (2012).
[14] T. Peyronel, O. Firstenberg, Q. Liang, S. Hofferberth, A. V. Gorshkov, T. Pohl, M. D. Lukin, and V. Vuletic, Nature **488**, 57 (2012).
[15] M. Mücke, E. Figueroa, J. Bochmann, C. Hahn, K. Murr, S. Ritter, C. J. Villas-Boas, and G. Rempe, Nature **465**, 755 (2010).
[16] T. Kampschulte, W. Alt, S. Manz, M. Martinez-Dorantes, R. Reimann, S. Yoon, D. Meschede, M. Bienert, and G. Morigi, Phys. Rev. A **89**, 033404 (2014).
[17] R. Röhlsberger, H.-C. Wille, K. Schlage, and B. Sahoo, Nature **482**, 199 (2012).
[18] P. R. Hemmer, A. V. Turukhin, M. S. Shahriar, and J. A. Musser, Opt. Lett. **26**, 361 (2001).

- [19] V. M. Acosta, K. Jensen, C. Santori, D. Budker, and R. G. Beausoleil, *Phys. Rev. Lett.* **110**, 213605 (2013).
- [20] G. B. Serapiglia, E. Paspalakis, C. Sirtori, K. L. Vodopyanov, and C. C. Phillips, *Phys. Rev. Lett.* **84**, 1019 (2000).
- [21] B. S. Ham, P. R. Hemmer, and M. S. Shahriar, *Opt. Comm.* **144**, 227 (1997).
- [22] A. V. Turukhin, V. S. Sudarshanam, M. S. Shahriar, J.A. Musser, B. S. Ham, and P. R. Hemmer, *Phys. Rev. Lett.* **88**, 023602 (2001).
- [23] J. J. Longdell, E. Fraval, M. J. Sellars, and N. B. Manson, *Phys. Rev. Lett.* **95**, 063601 (2005).
- [24] E. Baldit, K. Bencheikh, P. Monnier, S. Briauudeau, J.A. Levenson, V. Crozatier, I. Lorgeré, F. Bretenaker, J. L. Le Gouët, O. Guillot-Noël, and Ph. Goldner, *Phys. Rev. B* **81**, 144303 (2010).
- [25] G. Heinze, C. Hubrich, and T. Halfmann, *Phys. Rev. Lett.* **111**, 033601 (2013).
- [26] L. Jiang, H. Pu, W. Zhang, and H., Y. Ling, *Phys. Rev. A* **80**, 033606 (2009).
- [27] H. H. Jen and Daw-Wei Wang, *Phys. Rev. A* **87**, 061802(R) (2013).
- [28] H. H. Jen and Daw-Wei Wang, *J. Opt. Soc. Am. B* **31**, 2931 (2014).
- [29] R. H. Lehmburg, *Phys. Rev. A* **2**, 883 (1970).
- [30] R. H. Dicke, *Phys. Rev.* **93**, 99 (1954).
- [31] M. Gross and S. Haroche, *Phys. Rep.* **93** 301 (1982).
- [32] S. L. Bromley, B. Zhu, M. Bishof, X. Zhang, T. Bothwell, J. Schachenmayer, T. L. Nicholson, R. Kaiser, S. F. Yelin, M. D. Lukin, A. M. Rey, and J. Ye, *Nat. Commun.* **7**:11039 (2016).
- [33] W. Guerin, M. O. Araújo, and R. Kaiser, *Phys. Rev. Lett.* **116**, 083601 (2016).
- [34] Y. Sonnefraud, N. Verellen, H. Sobhani, G. A.E. Vandenbosch, V. V. Moshchalkov, P. V. Dorpe, P. Nordlander, and S. A. Maier, *ACS Nano* **4**, 1664 (2010).
- [35] B. H. McGuyer, M. McDonald, G. Z. Iwata, M. G. Tarallo, W. Skomorowski, R. Moszynski, and T. Zelevinsky, *Nat. Phys.* **11**, 32 (2015).
- [36] S. D. Jenkins, J. Ruostekoski, N. Papisimakis, S. Savo, and N. I. Zheludev, *Phys. Rev. Lett.* **119**, 053901 (2017).
- [37] R. Röhlsberger, K. Schlage, B. Sahoo, S. Couet, and R. Rüffer, *Science* **328**, 1248 (2010).
- [38] J. Keaveney, A. Sargsyan, U. Krohn, I. G. Hughes, D. Sarkisyan, and C. S. Adams, *Phys. Rev. Lett.* **108**, 173601 (2012).
- [39] Z. Meir, O. Schwartz, E. Shahmoon, D. Oron, and R. Ozeri, *Phys. Rev. Lett.* **113**, 193002 (2014).
- [40] J. Pellegrino, R. Bourgain, S. Jennewein, Y. R. P. Sortais, A. Browaeys, S. D. Jenkins, and J. Ruostekoski, *Phys. Rev. Lett.* **113**, 133602 (2014).
- [41] S. Jennewein, M. Besbes, N. J. Schilder, S. D. Jenkins, C. Sauvan, J. Ruostekoski, J.-J. Greffet, Y. R. P. Sortais, and A. Browaeys, *Phys. Rev. Lett.* **116**, 233601 (2016).
- [42] S. D. Jenkins, J. Ruostekoski, J. Javanainen, R. Bourgain, S. Jennewein, Y. R. P. Sortais, and A. Browaeys, *Phys. Rev. Lett.* **116**, 183601 (2016).
- [43] S. J. Roof, K. J. Kemp, M. D. Havey, and I. M. Sokolov, *Phys. Rev. Lett.* **117**, 073003 (2016).
- [44] M. H. Oliveira, C. E. Máximo, and C. J. Villas-Boas, *arXiv:2104.00761v3*.
- [45] R. Kubo, *J. Phys. Soc. Jap. Vol.* **17**, 1100 (1962).
- [46] S. Sevinçli, N. Henkel, C. Ates, and T. Pohl, *Phys. Rev. Lett.* **107**, 153001 (2011).
- [47] H. H. Jen, M.-S. Chang, and Y.-C. Chen, *Phys. Rev. A* **94**, 013803 (2016).
- [48] H. H. Jen, *Phys. Rev. A* **96**, 023814 (2017).
- [49] L. Chomaz, L. Corman, T. Yefsah, R. Desbuquois, and J. Dalibard, *New J. Phys.* **14**, 055001 (2012).
- [50] F. Andreoli, M. J. Gullans, A. A. High, A. Browaeys, and D. E. Chang, *Phys. Rev. X* **11**, 011026 (2021).
- [51] N. E. Rehler and J. H Eberly, *Phys. Rev. A* **3**, 1735 (1971).
- [52] I. E. Mazets and G. Kurizski, *J. Phys. B* **40**, F105 (2007).
- [53] M. O. Scully, *Phys. Rev. Lett.* **102**, 143601 (2009).
- [54] H. H. Jen, *Ann. of Phys. (N.Y.)* **360**, 556 (2015).
- [55] D. Petrosyan, J. Otterbach, and M. Fleischhauer, *Phys. Rev. Lett.* **107**, 213601 (2011).
- [56] A. Asenjo-Garcia, M. Moreno-Cardoner, A. Albrecht, H. J. Kimble, D. E. Chang, *Phys. Rev. X* **7**, 031024 (2017).
- [57] M. O. Scully and M. S. Zubairy, *Quantum Optics* (Cambridge University Press, 1997).
- [58] S.-S. Hsiao, K.-T Chen, and I. A. Yu, *Opt. Express* **28**, 28414 (2020).
- [59] B. Kim, *et al.*, *Commun. Phys.* **4**, 101 (2021).
- [60] P. Bienias, *et al.*, *Phys. Rev. Res.* **2**, 033049 (2020).
- [61] A. Tebben, *et al.*, *Phys. Rev. A* **103**, 063710 (2021).
- [62] C. Cohen-Tannoudji, J. Dupont-Rock, and G. Grynberg, *Atom-photon interactions: Basic processes and applications* (John Wiley & Sons, 1992).
- [63] O. Morice, Y. Castin, and J. Dalibard, *Phys. Rev. A* **51**, 3896 (1995).
- [64] M.-T. Rouabah, M. Samoylova, R. Bachelard, P. W. Courteille, R. Kaiser, and N. Piovella, *JOSA A* **31**, 1031 (2014).
- [65] L. Corman, J. L. Ville, R. Saint-Jalm, M. Aidelsburger, T. Bienaimé, S. Nascimbène, J. Dalibard, and J. Beugnon, *Phys. Rev. A* **96**, 053629 (2017).